Patterns and excitations in antiferromagnetic spinor condensates

Michał Matuszewski,[1] Kai Bongs,[2] and Jochen Kronjäger[2]
[1]*Instytut Fizyki PAN, Aleja Lotników 32/46, 02-668 Warsaw, Poland,*
[2]*MUARC, School of Physics and Astronomy, University of Birmingham, Edgbaston, Birmingham B15 2TT, United Kingdom*
(Received 21 December 2011; published 27 February 2012)

We consider the phenomenon of spin-pattern formation reported in recent experiments in spin-2 rubidium condensate [J. Kronjäger, C. Becker, P. Soltan-Panahi, K. Bongs, and K. Sengstock, Phys. Rev. Lett. **105**, 090402 (2010)]. To understand the mechanism underlying the process and explain the parameters such as pattern period and growth rate, we employ the Bogoliubov–de Gennes equations and an alternative method based on energy conservation and the uncertainty principle. While the two methods agree in the spin-1 case, only the second method can provide analytical results in the spin-2 case. Using these results, we explain the occurrence of two regimes, the spin-dominated and the Zeeman-dominated, with the prevalence of spin-wave modes and quadrupole modes, respectively. We obtain very good agreement between theory and experiment for the pattern period and growth rate over several orders of magnitude of the magnetic field strength.

DOI: 10.1103/PhysRevA.85.023635 PACS number(s): 03.75.Lm, 05.30.Jp, 32.60.+i, 67.85.−d

I. INTRODUCTION

Spinor condensates have emerged as a promising quantum model system for spontaneous structure formation and symmetry breaking [1–6]. As such they were proposed to offer links to a broad range of fields, for example, the emergence of density variations in the universe via the Kibble-Zurek mechanism [7–9]. The instabilities associated with symmetry breaking have been shown to amplify quantum noise [10–13] and have recently been used to generate large numbers of entangled atom pairs [14–16].

The emergence of structure in the ferromagnetic phase of $F = 1$ ^{87}Rb Bose-Einstein condensates [1,7–11,17–23] is intuitively linked to the formation of magnetic domains. Perhaps surprisingly, recent experiments have shown that pattern formation also occurs in antiferromagnetic systems [3,4,24]. Although these patterns emerge as unstable modes of the Gross-Pitaevskii equation, detailed numerical calculations are required in each case, and a generic understanding of the phenomenon is still lacking. In this article we present a physical interpretation linking the observed patterns to natural spinor order parameters and develop a simple general scheme allowing generation of approximate analytical formulas for key parameters such as pattern periodicity and growth rate. We focus on the homogeneous one-dimensional case as described in Ref. [4].

This article is organized as follows: After introducing the spinor Hamiltonian we test a physical interpretation of the observed patterns against a solution of the Bogoliubov equations for the $F = 1$ case. Following this we propose a general, spin-independent solution scheme based on energy and uncertainty considerations and demonstrate that it delivers the exact solution for the spin-1 case and a good approximation for spin-2.

II. MODEL

The Hamiltonian of a spinor Bose-Einstein condensate can be written as $\hat{H} = \hat{H}_0 + \hat{H}_A$, where the symmetric (spin-independent) part is

$$\hat{H}_0 = \sum_{j=-F\cdots+F} \int d\mathbf{r}\, \hat{\psi}_j^\dagger \left(-\frac{\hbar^2}{2m}\nabla^2 + \frac{c_0}{2}\hat{n} + V(\mathbf{r}) \right) \hat{\psi}_j, \quad (1)$$

where the subscripts $j = -F \cdots + F$ denote sublevels with magnetic quantum numbers along the z axis $m_f = j$, m is the atomic mass, $\hat{n} = \sum \hat{n}_j = \sum \hat{\psi}_j^\dagger \hat{\psi}_j$ is the total atom density, and $\hat{\psi} = (\hat{\psi}_{-F}, \ldots, \hat{\psi}_F)$. We will consider a Bose-Einstein condensate in a cigar-shaped trap elongated in the z direction, $V(\mathbf{r}) = \frac{1}{2}m\omega_\perp^2(x^2 + z^2) + \frac{1}{2}m\omega_z^2 z^2$. In the case of a spin-1 condensate, the asymmetric part of the Hamiltonian is [25]

$$\hat{H}_A = \int d\mathbf{r} \left(\sum_{j=-1,0,+1} E_j \hat{n}_j + \frac{c_1}{2} : \hat{\mathbf{F}}^2 : \right), \quad (2)$$

whereas in the spin-2 case, the asymmetric part can be written as [26]

$$\hat{H}_A = \int d\mathbf{r} \left(\sum_{j=-2\cdots+2} E_j \hat{n}_j + \frac{c_1}{2} : \hat{\mathbf{F}}^2 : + \frac{c_2}{2} \hat{\Theta}^\dagger \hat{\Theta} \right), \quad (3)$$

where E_j are the Zeeman energy levels, the spin density is $\hat{\mathbf{F}} = (\hat{\psi}^\dagger F_x \hat{\psi}, \hat{\psi}^\dagger F_y \hat{\psi}, \hat{\psi}^\dagger F_z \hat{\psi})$ where $F_{x,y,z}$ are the spin matrices, and the singlet pair operator is $\Theta = 2\psi_2\psi_{-2} - 2\psi_1\psi_{-1} + \psi_0^2$. In the above we assumed that the magnetic field is parallel to the z axis.

The linear part of the Zeeman effect induces a homogeneous rotation of the spin vector around the direction of the magnetic field. Since the Hamiltonian is invariant with respect to spin rotations around the z axis, we can remove this trivial effect by introducing a rotating frame for the spin oscillating with the Larmor frequency. We thus consider only the effect of the quadratic Zeeman shift [25]. For a sufficiently weak magnetic field we can approximate it by an energy shift of the $m_f = \pm 1$ (and $m_f = \pm 2$) sublevels, $\Delta E_j = j^2 \delta E$, where $\delta E \approx \pm\alpha^2 E_{\mathrm{HFS}}/16$, E_{HFS} is the hyperfine energy splitting at zero magnetic field, $\alpha = (g_I + g_J)\mu_B B / E_{\mathrm{HFS}}$, μ_B is the Bohr magneton, g_I and g_J are the gyromagnetic ratios of electron

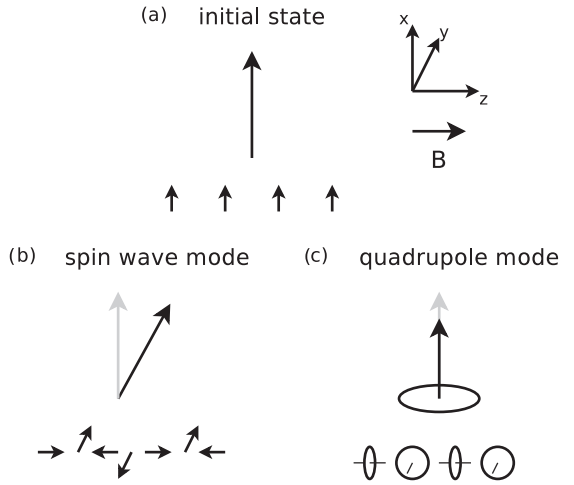

FIG. 1. (a) The initial state of the condensate is polarized transversely to the magnetic field (TP) and corresponds to an energy maximum. Two modes can destabilize the condensate in the presence of magnetic field: (a) the spin-wave (SW) mode, which tilts the spin vector and gives rise to the pattern with alternating spin directions, and (b) the quadrupole mode (QM), which reduces the spin vector and builds up the nematic order parameter depicted by a disk with the axis determining the nematic direction.

and nucleus, and B is the magnetic field strength [25]. We note that δE can be positive or negative depending on whether we consider the lower or the upper hyperfine level, but in both cases it is proportional to the square of the magnetic field strength B. Splitting δE with arbitrary sign can be alternatively induced using optical [27] or microwave [13,28] fields.

III. SPIN-1 CASE

In a recent experiment with an antiferromagnetic spin-2 rubidium condensate, a striking feature of regular pattern formation was observed [4]. The condensate was initially prepared in the transversely polarized (TP) state, depicted schematically in Fig. 1(a). If the condensate was placed in a sufficiently strong magnetic field, periodic spin patterns, depicted in Fig. 2, developed after a certain time of evolution. Remarkably, the patterns were clearly different in the two

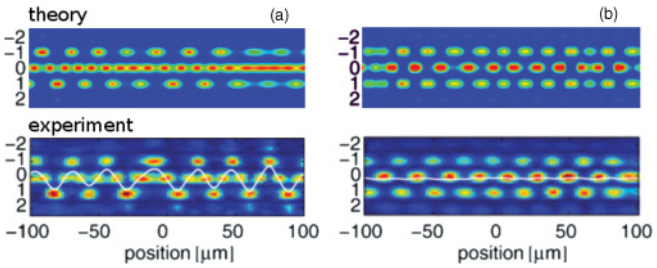

FIG. 2. (Color online) Examples of density profiles of spin components in spontaneous patterns of $F = 2$ ^{87}Rb: (a) spin-wave pattern at $B = 0.25$ G, and (b) quadrupole wave pattern at $B = 1.1$ G. The figures in the top row show the results of numerical simulations within the truncated Wigner approximation, while the bottom row shows the experimental data. The trap frequencies are $\omega_{x,y,z} = 2\pi \times (85,133,0.8)$ Hz and the atom density in the center of the trap (magnified here) is $n_0 = 8.1 \times 10^{13}$ per cm^3.

regimes, corresponding to a weak and strong magnetic field. Below, we will explain the emergence of the two regimes by using a simple analytical model and provide a tool to calculate some basic characteristics of the pattern formation, such as pattern period and instability growth rate. For this purpose, we will first consider a simpler spin-1 model and show that a similar phenomenon can occur equally well here, provided that the quadratic Zeeman shift δE is negative.

For an antiferromagnetic condensate in the absence of magnetic field, the initial TP state is a stable, although maximally spin-excited state. This is because of spin conservation, which ensures that the condensate remains maximally polarized in the transverse direction [29]. The situation changes after introducing the magnetic field, which breaks the transverse spin conservation.

In the spin-1 model, there are generally three different excitation modes, i.e., the density wave mode, spin-wave mode (SW), and the quadrupole mode (QM) [30,31]. While the density wave mode is always stable due to strong repulsive atomic interactions, the spin-wave mode and the quadrupole mode may become unstable in the presence of a magnetic field. In contrast to the case of a $F = 1/2$ system, where a coherent quantum state can be described using a single spin vector on the Bloch sphere, the $F = 1$ system is only fully described by a pair of one spin vector and one nematic order parameter [32]. Using this language, Figs. 1(b) and 1(c) schematically show the action of excitation modes on the TP state (top), together with the final spin patterns (bottom). By looking carefully at the experimental spin patterns [4], one can see that the spin-wave pattern develops in a weak magnetic field (interaction regime) [see Fig. 2(a)], while the quadrupole pattern develops in the Zeeman-dominated regime [see Fig. 2(b)].

It is possible to understand this behavior qualitatively by considering the instability growth rates of the SW modes and QMs as a function of the quadratic Zeeman splitting δE. The SW modes are unstable for $\delta E < 0$, because only in this case does tilting the spin vectors toward the magnetic field axis while keeping the spin density $|\mathbf{F}|$ constant reduce the quadratic Zeeman energy (2). We can thus expect that the instability of SW modes will grow linearly with $(-\delta E)$. On the other hand, QMs are unstable for both positive and negative δE, because the reduction of the spin density $|\mathbf{F}|$ always reduces the energy for $c_1 > 0$. At the same time, they must be stable at $B = 0$. The growth rates of QMs can then be only quadratic in δE. Consequently, we can expect that the SW modes will be dominant unstable modes for small negative δE, but QMs may become dominant at higher magnetic fields. On the other hand, for positive δE, QMs are the only unstable modes.

A. Bogoliubov mode analysis

We support this reasoning with analytical calculations of linearized Bogoliubov modes of a homogeneous $F = 1$ condensate. The linear excitation modes are solutions of the Bogoliubov–de Gennes equations [33] around a stationary state, $\psi_j(x,t) = \sqrt{n_j}\exp(-i\mu_j t) + \delta\psi_j(\mathbf{r},t)$, where

$$\delta\psi_j(\mathbf{r},t) = (u_j e^{i\mathbf{k}\cdot\mathbf{r}-i\omega t} + v_j^* e^{-i\mathbf{k}\cdot\mathbf{r}+i\omega^* t})e^{-i\mu_j t} \qquad (4)$$

is a small perturbation.

In general, the initial TP state is not an eigenstate of the Hamiltonian. However, in weak magnetic fields, it can be well approximated with the phase-matched (PM) stationary (inert) state [25], which becomes equivalent to the TP state at $B = 0$. On the other hand, in strong magnetic fields when the rotating wave approximation can be applied [4], the TP state becomes an exact eigenstate of the Hamiltonian. In this limit we can calculate its excitation modes directly.

In the limit $c_1 \ll c_0$, the excitation of density modes requires much more energy than spin excitations. Here, we consider low-energy excitations only and can thus assume that the density profile of the condensate is practically unchanged, while the unstable spin modes can lead to the appearance of spin patterns. The growth rate of these patterns is determined by the most unstable mode, which grows exponentially at a rate $\kappa_{\max} = \max \Im(\omega)$. This rate and the corresponding wave-vector length $k_{\max}$, which corresponds to the pattern lattice constant, can be calculated analytically in the respective limits (here $\xi_s = \sqrt{2}\pi\hbar/\sqrt{mc_1 n}$ is the spin healing length and $\xi_B = \sqrt{2}\pi\hbar/\sqrt{m|\delta E|}$ is the magnetic healing length). For a phase-matched (PM) state in weak magnetic fields ($\delta E \ll c_1 n$), SW modes have

$$\kappa_{\max} = \frac{|\delta E|}{2\hbar}, \quad k_{\max} = \frac{\sqrt{2}\pi}{\xi_B} \quad \text{for} \quad \delta E < 0,$$
$$\kappa_{\max} = 0 \text{ (stable)} \quad \text{for} \quad \delta E \geqslant 0, \tag{5}$$

while QMs have

$$\kappa_{\max} = \frac{\delta E^2}{4\hbar c_1 n}, \qquad k_{\max} = \frac{\pi}{\xi_s}\sqrt{8 - \left(\frac{\delta E}{c_1 n}\right)^2}. \tag{6}$$

In strong magnetic fields ($\delta E \gg c_1 n$), we consider excitations of the TP state. It turns out that in this regime SW modes are always stable, while QMs have

$$\kappa_{\max} = \frac{c_1 n}{2\hbar}, \qquad k_{\max} = \frac{\sqrt{2}\pi}{\xi_s}. \tag{7}$$

Figure 3 shows the dependence of the maximum growth rate $\kappa_{\max}$ and the corresponding pattern wave vectors $k_{\max}$ of PM and TP states in the appropriate regimes. Additionally, the dashed-dotted line shows the overlap of the PM state and the initial TP state, $A = (1/N)\sum_j |\psi_j^{*(\mathrm{PM})}\psi_j^{(\mathrm{TP})}|$. It gives a measure of the applicability of the weak magnetic field assumption. We also note that the PM state exists only up to $|\delta E|/c_1 n = (B/B_0)^2 = 2$ [25].

While the spin-wave modes dominate the instability in weak magnetic fields, and their maximal growth rate increases linearly with δE (quadratically with the magnetic field strength), it becomes stable in the regime of strong magnetic field, where the quadrupole mode is the only unstable mode. In between, we expect a crossover region where the two modes compete, which can result in the appearance of irregular patterns. The wave-vector length of the pattern grows linearly with the magnetic field at low B, but it saturates in strong magnetic field, in agreement with the experimental data [4].

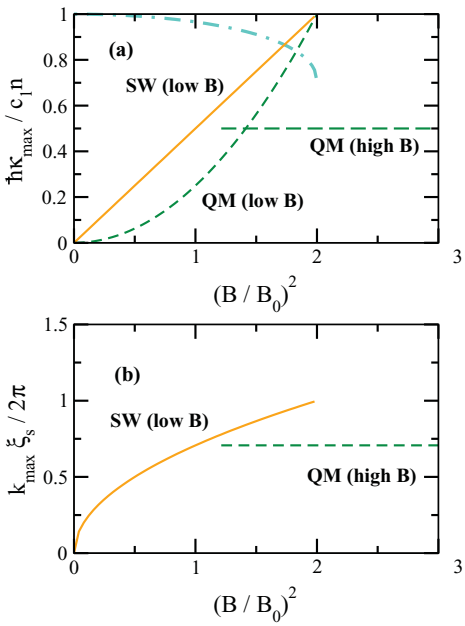

FIG. 3. (Color online) (a) Analytical results for the dependence of the maximum growth rate of SW modes and QMs in the function of magnetic field. The figures correspond to a spin-1 Bose-Einstein condensate with a negative quadratic Zeeman splitting $\delta E < 0$. The "low B" lines correspond to the PM eigenstate [25], which is close to the initial TP state in weak magnetic field, and "high B" lines correspond to the exact initial TP state in the limit of strong magnetic field. B_0 denotes the magnitude of the magnetic field for which the interaction and Zeeman energies are equal, $|\delta E| = c_1 n$. The dashed-dotted line shows the overlap of the PM state and the initial TP state, $A = (1/N)\sum_j |\psi_j^{*(\mathrm{PM})}\psi_j^{(\mathrm{TP})}|$. (b) The most unstable wave vector $k_{\max}$ as a function of B/B_0.

B. Energy conservation and the uncertainty principle

We now present an alternative method of calculating the growth rate and the wave-vector length of the most unstable mode. The method is based on the energy conservation law and the uncertainty principle. In contrast to the Bogoliubov method, it can be used to obtain approximate analytical formulas also in the case of higher-F systems.

In the limit of a homogeneous condensate, the initial TP state can be described by the spinor [30,31]:

$$\zeta_{\mathrm{TP}} = e^{i\phi}e^{-i\frac{\pi}{2}F_y}\begin{pmatrix}1\\0\\0\end{pmatrix} = e^{i\phi}\begin{pmatrix}1/2\\\sqrt{1/2}\\1/2\end{pmatrix}. \tag{8}$$

The kinetic, quadratic Zeeman, and interaction energies of this state are (per atom)

$$e_{\mathrm{TP}}^{\mathrm{kin}} = 0, \quad e_{\mathrm{TP}}^{\mathrm{Z}} = \frac{1}{2}\delta E, \quad e_{\mathrm{TP}}^{\mathrm{int}} = \frac{c_1}{2}n. \tag{9}$$

We neglect the influence of the spin-independent interaction energy, potential energy, and the linear Zeeman energy, which we assume to be constant. Now we consider the patterns created by the instability of the condensate. We are interested in the spin structure at the instant when the pattern is fully developed but is still a result of a growth of a single unstable mode depicted in Fig. 1(b) or 1(c). In the case of the spin-wave

mode, the spin vector, initially polarized along x, tilts in different directions in the y-z plane. We approximate the resulting spin pattern as a spin rotating in this plane as we move along z:

$$\zeta_{\mathrm{SW}} = e^{i\phi} e^{-i(k_{\mathrm{SW}} z+\phi_s)F_x} \begin{pmatrix} 1 \\ 0 \\ 0 \end{pmatrix}, \tag{10}$$

where k_{SW} is the wave vector of the spin pattern. The phases ϕ and ϕ_s can vary in different realizations of the experiment. The average energies per atom for this state are

$$e^{\mathrm{kin}}_{\mathrm{SW}} = \frac{\hbar^2 k^2_{\mathrm{SW}}}{4m}, \quad e^{\mathrm{Z}}_{\mathrm{SW}} = \frac{3}{4}\delta E, \quad e^{\mathrm{int}}_{\mathrm{SW}} = \frac{c_1}{2} n. \tag{11}$$

Since the total energy in the system has to be conserved, we can determine k_{SW}. We can also estimate the upper limit for the growth rate of the unstable mode using the uncertainty principle. Since the difference in energy of two levels ΔE can only lead to a change of the state of the system after time Δt such that $\Delta E \Delta t \geqslant \hbar$, the inverse time scale κ_{SW} can be estimated from the energy gained by a single atom driven by the instability as $\kappa_{\mathrm{SW}} \leqslant \Delta e/\hbar = \hbar k^2_{\mathrm{SW}}/2m$. We obtain

$$k_{\mathrm{SW}} = \frac{\sqrt{2}\pi}{\xi_{\mathrm{B}}}, \qquad \kappa_{\mathrm{SW}} \leqslant \frac{|\delta E|}{2\hbar}, \tag{12}$$

which agrees perfectly with the analysis of the Bogoliubov modes from the preceding section if we take κ_{SW} as the upper limit.

In a similar manner, we can approximate the pattern of the quadrupole wave with a rotated polar state [30,31]

$$\zeta_{\mathrm{QM}} = e^{i\phi} e^{-i(k_{\mathrm{QM}} z+\phi_s)F_x} \begin{pmatrix} 0 \\ 1 \\ 0 \end{pmatrix} \tag{13}$$

with the energies

$$e^{\mathrm{kin}}_{\mathrm{QM}} = \frac{\hbar^2 k^2_{\mathrm{QM}}}{2m}, \quad e^{\mathrm{Z}}_{\mathrm{QM}} = \frac{1}{2}\delta E, \quad e^{\mathrm{int}}_{\mathrm{QM}} = 0. \tag{14}$$

The resulting growth rate and wave-vector length of the pattern are

$$k_{\mathrm{QM}} = \frac{\sqrt{2}\pi}{\xi_{\mathrm{s}}}, \qquad \kappa_{\mathrm{QM}} \leqslant \frac{c_1 n}{2\hbar}, \tag{15}$$

and thus we again recover the result of the Bogoliubov analysis. We note that the density pattern given by Eq. (13) has in fact a period equal to π/k_{QM}, because the rotation by π only changes the sign of the spinor. However, at the early stages of the instability, the density maxima have the same phase, and $2\pi/k_{\mathrm{QM}}$ is the visible period. Small density maxima with opposite phase develop only later, but the system never truly gets to the state (13), due to the growth of other unstable modes.

IV. SPIN-2 CASE

In the case of a spin-2 condensate, the Bogoliubov analysis becomes problematic due to the difficulty in determining exact eigenstates in the case of a finite magnetic field. Encouraged by the results of the previous section, we apply the approximate calculations exploiting the energy conservation. Guided by the experimental and numerical data, we take the initial state and the generated spin patterns as

$$\begin{aligned} \zeta_{\mathrm{TP}} &= e^{i\phi} e^{-i\frac{\pi}{2}F_y}(1,0,0,0,0)^T, \\ \zeta_{\mathrm{SW}} &= e^{i\phi} e^{-i(k_{\mathrm{SW}} z+\phi_s)F_x}(1,0,0,0,0)^T, \\ \zeta_{\mathrm{QM}} &= e^{i\phi} e^{-i(\frac{k_{\mathrm{QM}}}{2} z+\phi_s)F_x}(0,\sqrt{1/2},0,\sqrt{1/2},0)^T, \end{aligned} \tag{16}$$

where we have taken into account that here the rotation of the ζ_{QM} state by π around the x axis renders the state unchanged, while the rotation by $\pi/2$ gives $-\zeta_{\mathrm{QM}}$ [34].

The resulting parameters of the most unstable modes are

$$\begin{aligned} k_{\mathrm{SW}} &= \frac{\sqrt{6}\pi}{\xi_{\mathrm{B}}}, \quad \kappa_{\mathrm{SW}} \leqslant \frac{3|\delta E|}{2\hbar}, \\ k_{\mathrm{QM}} &= \frac{\sqrt{2}\pi}{\xi_{\mathrm{s}}}, \quad \kappa_{\mathrm{QM}} \leqslant \frac{c_1 n}{2\hbar}. \end{aligned} \tag{17}$$

By the same arguments as in the spin-1 case, $2\pi/k_{\mathrm{QM}}$ is the period of the density pattern formed at early time.

In Fig. 4 we compare the above results with numerical simulations of a spin-2 Rb condensate. We simulated the evolution of a condensate in a periodic box in one dimension. To model the above quantum system numerically in an efficient way, we applied the truncated Wigner approximation [11,23,35] to describe the evolution. The initial state was perturbed by spectrally limited noise to account for quantum fluctuations and density profile imperfections [20,29]. We achieve a very good agreement between analytical, numerical, and experimental [36] results for both the wave-vector length

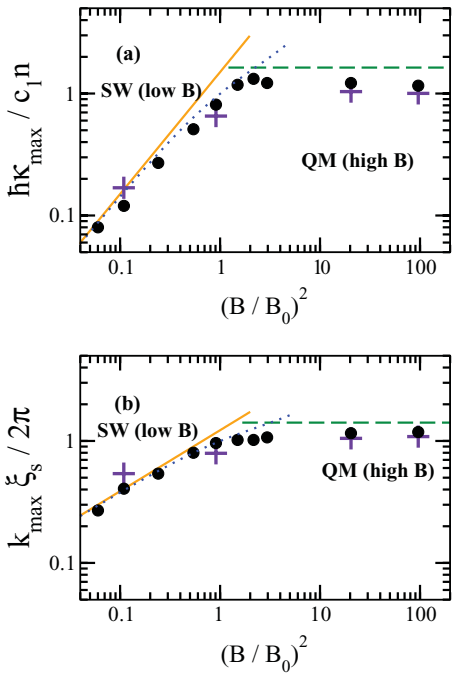

FIG. 4. (Color online) As in Fig. 3 but for a spin-2 condensate. Here we present both theoretical and experimental results on a bilogarithmic scale. The black dots depict the results of numerical simulations within the truncated Wigner approximation, and the crosses correspond to the experimental data. The lines are given by Eqs. (17). In addition, the dotted line represents a numerical Bogoliubov analysis [4].

and the growth rate over several orders of magnitude of the Zeeman to interaction energy ratio $(B/B_0)^2$. The agreement between the density profiles of the spin components is also very good (see examples in Fig. 2). We clearly observe the crossover from the SW dependence in weak magnetic field to the QM dependence in the Zeeman-dominated regime.

Finally, we comment on the possible sources of discrepancy between the analytical and experimental results. The numerical simulations (black dots in Fig. 4) agree very well with the experiment (crosses), as we checked using both a one-dimensional numerical code, including the harmonic trapping, and a code with no longitudinal trapping and periodic boundary conditions. On the other hand, the analytical curves deviate from the numerical and experimental, especially in the strong magnetic field limit (by about 10% for the pattern wavelength and about 20% for the growth rate). We argue that this discrepancy can be attributed to the imperfect overlap between the initial TP state and the stationary state, which are not the same in the spin-2 case. The overlap between the two is about 90%, and since the remaining part can be interpreted as an addition of $k = 0$ Bogoliubov modes of the stationary state, which are stable [4], we can expect that $k_{\max}$ and $\kappa_{\max}$ will be smaller than predicted using the assumption that the whole condensate is unstable. To support this conclusion, we have checked that in the spin-1 case, when the overlap between the TP state and the stationary state is perfect, the discrepancy between the analytical and numerical results is much smaller. Additionally, we note that another source of discrepancy could be the imperfect overlap between the true pattern and the rotating wave guess [Eq. (16)]. We checked that the overlap between the QM state (16) and the numerically obtained patterns is on average only about 75%, even when making an optimal choice of ϕ_s at each point in space. Taking this into account, we conclude that the method gives surprisingly accurate results in spite of the simplifications involved. We note that this method is rather general and could be used to describe phenomena other than the periodic pattern formation considered here.

V. CONCLUSIONS AND OUTLOOK

Linking the observed pattern formation to excitations of fundamental spinor order parameters and following the simple scheme we developed in this article leads to an intuitive analytical understanding of the physics involved in antiferromagnetic pattern formation in spinor condensates. The generality of the presented scheme opens a new avenue of understanding pattern formation in the currently emerging higher spin systems [37–42], for which a more rigorous Bogoliubov treatment is impractical. This offers new perspectives for investigations of nonequilibrium phenomena and the transition between quantum and classical spin systems.

ACKNOWLEDGMENTS

We thank Mariusz Gajda for stimulating discussions. This work was supported by the Foundation for Polish Science through the "Homing Plus" program. We thank EPSRC for support under Grants No. EP/E036473/1 and No. EP/H009914/1.

[1] L. E. Sadler, J. M. Higbie, S. R. Leslie, M. Vengalattore, and D. M. Stamper-Kurn, Nature (London) **443**, 312 (2006).
[2] M. Vengalattore, S. R. Leslie, J. Guzman, and D. M. Stamper-Kurn, Phys. Rev. Lett. **100**, 170403 (2008).
[3] C. Klempt, O. Topic, G. Gebreyesus, M. Scherer, T. Henninger, P. Hyllus, W. Ertmer, L. Santos, and J. J. Arlt, Phys. Rev. Lett. **103**, 195302 (2009).
[4] J. Kronjäger, C. Becker, P. Soltan-Panahi, K. Bongs, and K. Sengstock, Phys. Rev. Lett. **105**, 090402 (2010).
[5] M. Scherer, B. Lücke, G. Gebreyesus, O. Topic, F. Deuretzbacher, W. Ertmer, L. Santos, J. J. Arlt, and C. Klempt, Phys. Rev. Lett. **105**, 135302 (2010).
[6] M. Vengalattore, J. Guzman, S. R. Leslie, F. Serwane, and D. M. Stamper-Kurn, Phys. Rev. A **81**, 053612 (2010).
[7] B. Damski and W. H. Zurek, Phys. Rev. Lett. **99**, 130402 (2007).
[8] H. Saito, Y. Kawaguchi, and M. Ueda, Phys. Rev. A **76**, 043613 (2007).
[9] A. Lamacraft, Phys. Rev. Lett. **98**, 160404 (2007).
[10] G. I. Mias, N. R. Cooper, and S. M. Girvin, Phys. Rev. A **77**, 023616 (2008).
[11] J. D. Sau, S. R. Leslie, D. M. Stamper-Kurn, and M. L. Cohen, Phys. Rev. A **80**, 023622 (2009).
[12] C. Klempt, O. Topic, G. Gebreyesus, M. Scherer, T. Henninger, P. Hyllus, W. Ertmer, L. Santos, and J. J. Arlt, Phys. Rev. Lett. **104**, 195303 (2010).
[13] S. R. Leslie, J. Guzman, M. Vengalattore, J. D. Sau, M. L. Cohen, and D. M. Stamper-Kurn, Phys. Rev. A **79**, 043631 (2009).
[14] C. Gross, H. Strobel, E. Nicklas, T. Zibold, N. Bar-Gill, G. Kurizki, and M. K. Oberthaler, Nature (London) **480**, 219 (2011).
[15] B. Lücke, M. Scherer, J. Kruse, L. Pezze, F. Deuretzbacher, P. Hyllus, O. Topic, J. Peise, W. Ertmer, J. Arlt, L. Santos, A. Smerzi, and C. Klempt, Science **334**, 773 (2011).
[16] E. M. Bookjans, C. D. Hamley, and M. S. Chapman, Phys. Rev. Lett. **107**, 210406 (2011).
[17] W. Zhang, D. L. Zhou, M.-S. Chang, M. S. Chapman, and L. You, Phys. Rev. Lett. **95**, 180403 (2005).
[18] H. Saito and M. Ueda, Phys. Rev. A **72**, 023610 (2005).
[19] M. Uhlmann, R. Schützhold, and U. R. Fischer, Phys. Rev. Lett. **99**, 120407 (2007).
[20] H. Saito, Y. Kawaguchi, and M. Ueda, Phys. Rev. A **75**, 013621 (2007).
[21] Y. Kawaguchi, H. Saito, K. Kudo, and M. Ueda, Phys. Rev. A **82**, 043627 (2010).
[22] J. Sau, S. R. Leslie, M. Cohen, and D. M. Stamper-Kurn, New J. Phys. **12**, 085011 (2010).
[23] R. Barnett, A. Polkovnikov, and M. Vengalattore, Phys. Rev. A **84**, 023606 (2011).
[24] E. M. Bookjans, A. Vinit, and C. Raman, Phys. Rev. Lett. **107**, 195306 (2011).

[25] M. Matuszewski, T. J. Alexander, and Y. S. Kivshar, Phys. Rev. A **80**, 023602 (2009).
[26] C. V. Ciobanu, S.-K. Yip, and T.-L. Ho, Phys. Rev. A **61**, 033607 (2000).
[27] L. Santos, M. Fattori, J. Stuhler, and T. Pfau, Phys. Rev. A **75**, 053606 (2007).
[28] F. Gerbier, A. Widera, S. Fölling, O. Mandel, and I. Bloch, Phys. Rev. A **73**, 041602 (2006).
[29] M. Matuszewski, Phys. Rev. Lett. **105**, 020405 (2010).
[30] T.-L. Ho, Phys. Rev. Lett. **81**, 742 (1998).
[31] T. Ohmi and K. Machida, J. Phys. Soc. Jpn. **67**, 1822 (1998).
[32] R. Barnett, A. Turner, and E. Demler, Phys. Rev. Lett. **97**, 180412 (2006).
[33] A. Leggett, Rev. Mod. Phys. **73**, 307 (2001).
[34] The form of ζ_{QM} is in principle not unique but was chosen to give the best possible approximation to the experimental and numerical profiles, providing an intuitive interpretation of the mode.
[35] M. J. Steel, M. K. Olsen, L. I. Plimak, P. D. Drummond, S. M. Tan, M. J. Collett, D. F. Walls, and R. Graham, Phys. Rev. A **58**, 4824 (1998).
[36] The experimental values presented in Fig. 4 were obtained by reevaluating raw data used in Ref. [4], in particular, taking into account atom number variations between runs.
[37] A. Griesmaier, J. Werner, S. Hensler, J. Stuhler, and T. Pfau, Phys. Rev. Lett. **94**, 160401 (2005).
[38] L. Santos and T. Pfau, Phys. Rev. Lett. **96**, 190404 (2006).
[39] T. Lahaye, T. Koch, B. Fröhlich, M. Fattori, J. Metz, A. Griesmaier, S. Giovanazzi, and T. Pfau, Nature (London) **448**, 672 (2007).
[40] S. Müller, J. Billy, E. A. L. Henn, H. Kadau, A. Griesmaier, M. Jona-Lasinio, L. Santos, and T. Pfau, Phys. Rev. A **84**, 053601 (2011).
[41] B. Pasquiou, E. Maréchal, G. Bismut, P. Pedri, L. Vernac, O. Gorceix, and B. Laburthe-Tolra, Phys. Rev. Lett. **106**, 255303 (2011).
[42] T. Weber, J. Herbig, M. Mark, H.-C. Nägerl, and R. Grimm, Science **299**, 232 (2003).